

RESEARCH ARTICLE

Linear viscoelasticity, nonlinear rheology and applications of polyethylene terephthalate vitrimers

Wei Zhang | Xiang Cui | Hongdong Zhang | Yuliang Yang | Ping Tang 

State Key Laboratory of Molecular Engineering of Polymers, Department of Macromolecular Science, Fudan University, Shanghai, China

Correspondence

Ping Tang, State Key Laboratory of Molecular Engineering of Polymers, Department of Macromolecular Science, Fudan University, Shanghai 200433, China.

Email: pingtang@fudan.edu.cn

Funding information

National Natural Science Foundation of China, Grant/Award Numbers: 21973017, 21774027, 21534002

Abstract

To enhance mechanical properties and processing performance of poly(ethylene terephthalate) (PET), it was upcycled to processable PET vitrimers with different crosslinking degrees by introducing dynamic network. The thermodynamics and linear viscoelasticity of PET vitrimers were explored by non-isothermal crystallization, isothermal sweep, frequency sweep and stress relaxation after incorporation of network. In particular, rheology experiments are sensitive to network structure and bond exchange mechanism in vitrimers. The pseudo-master curves show that relaxation processes are composed of three characteristic regions: Rouse-type relaxation of network strands, rubbery plateau and terminal relaxation of network, which is consistent with reversible gelation (RG) model. Two distinct (flow and chemical reaction) activation energies, are obtained by time-temperature superposition principle due to different temperature dependences of two relaxation behaviors. In addition, nonlinear rheology of PET vitrimers was investigated by extensional flow and start-up shear at the same Weissenberg number, and obvious strain hardening behavior were observed in all vitrimers. However, vitrimers with different crosslinking density exhibited distinct strain hardening trends as increase of extensional rate, corresponding to the ductility of material. On the basis of kinetics study, self-repairing and welding properties are further quantitatively explored for industrial applications.

KEY WORDS

dynamics, polyethylene terephthalate, rheology, vitrimer

1 | INTRODUCTION

PET is the most common thermoplastic polymer resin of polyesters with extensive applications in non-engineering plastics field, such as films, sheets and fibers,^{1–6} due to its low oxygen permeability and cost efficiency. However, PET is rarely applied in electronic appliances, machinery industry, or as other engineering plastics, which is attributed to the following two drawbacks.^{7,8} On one hand, the molecular weight of PET is relatively low and particularly

will be decreased from chain scission of severe degradation after manufacturing, resulting in deteriorated mechanical properties. On the other hand, the viscosity of PET will drop rapidly above melting temperature, leading to quite low melt strength and difficulties in the processing of foaming, blowing, thermoforming, etc.^{9–12} To make up for these shortcomings, a large number of fillers such as inorganic nanoparticles,^{13,14} organic metal salt¹⁵ and ionomers^{16–19} have been incorporated in PET to advance its mechanical properties. However, this strategy

only has a weak influence on enhancing the performance of PET by improving crystallization property.

Recently, Qiu et al. successfully transformed PET to continuously processable vitrimers by introducing dynamic network through industrial extruder.²⁰ Vitrimers, first proposed by Leibler,²¹ are a new kind of cross-linked polymer materials with dynamic network, namely the crosslinking points in network can be connected and disconnected to rearrange network topology by dynamic covalent bonds. The rearrangement is conducted by chemical reaction, such as transesterification,^{22–24} disulfide,^{25–27} dioxaborolane,²⁸ etc. Vitrimers combine the advantages of thermosets and thermoplastics simultaneously, because they exhibit outstanding physical properties like thermosets at low temperatures, and show excellent flow properties like thermoplastics at high processing temperatures.^{29,30} The interesting reaction kinetics of symmetric vitrimers have been examined by Chen et al., indicating two distinct relaxation mechanisms: Rouse-type relaxation of strands and network relaxation.³¹ The creep resistance and crosslinking degree were investigated by Qiu's work, confirming excellent processability of PET vitrimers.²⁰ The theory and simulation study with regard to dynamic network structures have been investigated in detail by our group.^{32–35} However, rheology behavior of PET vitrimers in experiments such as different mechanisms in the whole relaxation process, especially nonlinear rheology of vitrimers, has not been explored rigorously so far. Though this PET system is not perfect for research of vitrimer dynamics due to difficulty in characterization of detailed chemical structure, high-performance PET with excellent processability has an enormous potential in industry.

In this work, we upcycled PET to its vitrimers with different crosslinking degree by combining diepoxy and polyol of tertiary amine structure after melt compounding. It is demonstrated that the dynamic network was incorporated to PET successfully by thermodynamics and reaction kinetics study of PET vitrimers. On account of sensitivity of rheology to specific dynamic network structure, linear and nonlinear rheology experiments are applied in dynamics analysis of PET vitrimers, which is beneficial to the guidance on practical application. From pseudo-master curves by time-temperature superposition (TTS), the relaxation processes in linear viscoelasticity (LVE) region are guided by two distinct mechanisms: Rouse-type relaxation of network strands and terminal relaxation of dynamic network. The LVE rheology behaviors are consistent with scaling law in reversible gelation model,³⁶ including different relaxation mechanisms with different temperature dependences. In nonlinear rheology experiments, all PET vitrimers exhibited strain hardening under extensional flow, and the ductility

of material is closely associated with network density. Besides, applications are further expanded on the basis of dynamics study, such as self-repairing and welding properties of polymer interfaces, aiming to establish the relationship between structure and practical applications.

2 | EXPERIMENTAL SECTIONS

2.1 | Materials

PET (WK811) pellets with an intrinsic viscosity of 0.79 dL/g were provided by Wankai New Material Co., Ltd., China. 2,2-Bis(hydroxymethyl)-2,2',2"-nitrilotriethanol (BIS-TRIS, 98%, Aladdin), diglycidyl ether of bisphenol A (DGEBA, D.E.R. 332, Sigma-Aldrich), and an antioxidant (Irganox 1010, BASF) were used without further purification. PET811 pellets were dried at 110°C for 24 h under vacuum to prevent hydrolysis.

2.2 | Synthesis and characterization

2.2.1 | Preparation of PET vitrimers

The unentangled PET vitrimers were prepared by melting compounding at 270°C with BIS-TRIS, D.E.R. 332 and antioxidant in a torque rheometer (Changkai CTR-300, China) at a rotor speed of 60 rpm for 4 min. Then the obtained samples were post cured at 210°C for at least 72 h under vacuum to achieve completely cured PET vitrimers. The feed compositions of PET vitrimers are listed in Table 1 (the values indicate weight %). Branching agent BIS-TRIS (polyol with tertiary amine structure) was used to break up PET chains to incorporate more reactive groups into PET chains, and also as the catalyst. Crosslinking agent DER332 (diepoxy) was also introduced to crosslink the activated PET chains by the reaction between hydroxy groups (from the free polyol and from ring-opening of the epoxy) and ester groups from the PET backbone. The whole chemical reaction process is illustrated in Figure S1 based on Qiu's work,²⁰ and the curing degrees of samples depend on curing time. All PET vitrimers in subsequent characterization are

TABLE 1 The feed compositions of PET vitrimers (the values indicate weight %).

Sample	BIS-TRIS	DER332	Irganox	[OH]/[epoxy]
811-1.5	1%	1.5%	0.05%	2.7
811-2.5	1%	2.5%	0.05%	1.6
811-4.5	1%	4.5%	0.05%	0.9

completely cured through the preparation method above, except for the samples in isothermal rheology sweeps. PET vitrimers were prepared by injection molding at 270°C for all rheology characterization (linear and nonlinear) and self-repairing applications.

2.2.2 | Differential scanning calorimetry (DSC)

The crystallization and melting behaviors of PET and PET vitrimers were analyzed by non-isothermal process with DSC Q2000 (TA instruments) in nitrogen atmosphere. 8–10 mg of amorphous samples were heated from room temperature to 285°C and samples were then cooled to room temperature at heating/cooling rate of 10°C/min. Samples were heated to 285°C and maintained for 5 min to erase the previous thermal history, and subsequently quenched in liquid nitrogen to acquire amorphous state.¹³

2.2.3 | Thermogravimetric analyzer (TGA)

The thermal stability behavior of PET vitrimers were characterized by using TGA (Pyris1, PerkinElmer instrument).

2.2.4 | Tensile testing

The welding properties of vitrimer interfaces were measured by electronic universal testing machine Instron 5966, and the results are the average of at least five measurements per sample.

2.3 | Rheology

The LVE rheological behavior of PET vitrimers was observed at a TA Instruments ARES-G2 strain-controlled

rheometer, equipped with 25 mm parallel plates in nitrogen atmosphere. The isothermal curing process of cross-linking reaction was monitored at a frequency of 1 Hz with a strain amplitude of 3%, which is assured in the LVE region. The small amplitude oscillation shear frequency sweeps were performed from 100 to 0.1 Hz in the temperature range from 270 to 350°C, at 10°C each step with 3% strain, to construct pseudo-master curves by TTS principle. A continuous relaxation spectrum was converted directly from frequency sweep curves by software Trios. Stress relaxation measurements of PET vitrimers with different crosslinking density were conducted at the same strain from 270 to 350°C. The transient stress growth behavior of PET vitrimers was determined at strain rates of 0.05–4 s⁻¹ at fixed temperatures. All rheology data were acquired by actual measurements without extrapolation.

Uniaxial extension measurements were performed at ARES-G2 rheometer equipped with an extensional viscosity fixture (EVF), and the maximum achievable Hencky strain is 4.

3 | RESULTS AND DISCUSSION

3.1 | Thermal behavior

To investigate the thermal behavior of PET vitrimers, DSC experiments were carried out to probe thermal characteristics, such as glass transition temperature T_g , cold-crystallization temperature T_{cc} and melt-crystallization temperature T_{mc} . The DSC non-isothermal curves of neat PET and PET vitrimers are shown in Figure 1 and thermal parameters are summarized in Table 2. T_{cc} and melting temperature T_m can be characterized from the heating curve in Figure 1A, while T_{mc} is obtained from the cooling curve in Figure 1B. The introduction of network in PET vitrimers enhances T_g due to restriction to segmental motion of PET chain. Besides, T_g was

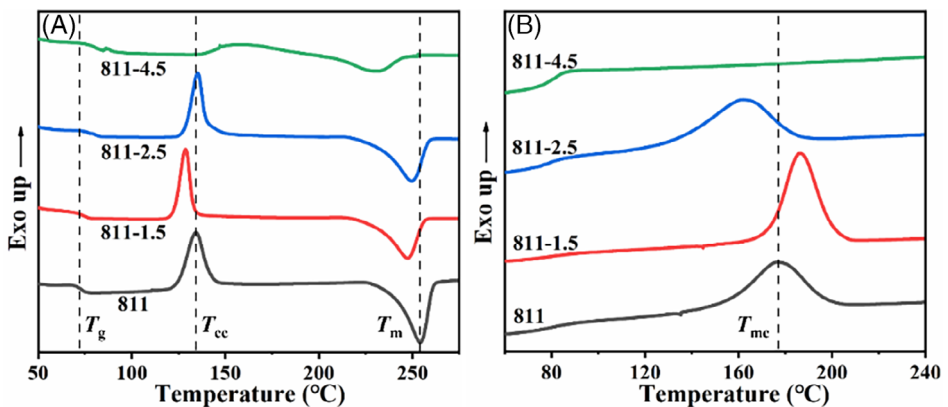


FIGURE 1 Non-isothermal behaviors of PET-811 and PET vitrimers: (A) heating curve, (B) cooling curve at rate of 10°C/min. The dashed lines are based on the characteristic temperatures of neat 811 samples.

TABLE 2 Non-isothermal melt and crystallization parameters results of PET and vitrimers.

Samples	T _g (°C)	T _{cc} (°C)	T _m (°C)	T _{mc} (°C)
PET811	72.8	133.7	254.3	176.2
811-1.5	73.9	128.8	247.2	186.7
811-2.5	78.5	135.5	249.6	162.0
811-4.5	82.7	157.5	230.7	-

advanced continuously with the increase of crosslinking agent contents from 811-1.5 to 811-4.5 samples. For 811-4.5 with the highest crosslinking degree, T_g was increased by about 10°C compared to neat PET 811, and 811-4.5 exhibited better thermal stability.

PET is a typical semi-crystalline polymer that the functionalization of chain mostly occurs in amorphous domain without affecting the distribution of crystalline region.³⁷ It is interesting that there are two opposition factors with the addition of crosslinking agent (DER). When the content of DER is small, T_{cc} and T_{mc} of 811-1.5 vitrimer shifted to lower temperature and higher temperature, respectively.³⁸ It is demonstrated that crosslinking points of network may act as heterogeneous nucleation sites for crystallization, thus accelerating the crystallization process. For 811-1.5, T_{mc} was increased by 10°C compared to neat PET-811, due to low crosslinking density of 811-1.5. However, T_{cc} became higher and T_{mc} became lower in 811-2.5, and T_{mc} even disappeared in 811-4.5, suggesting that crystallization ability was weakened with further addition of DER. The segmental alignment is disrupted by crosslinking constraints and the crosslinked microdomain places a physical barrier to be surrounded for chain packing. The non-monotonic change of T_{mc} results from the competition between heterogeneous nucleation by branching points and slowing down of chain dynamics (growth rate in crystallization) due to increase in crosslinking density. A suitable density of crosslinking points plays a dominant role by providing heterogeneous nucleation sites to enhance crystallization ability.

3.2 | Linear viscoelasticity

3.2.1 | Isothermal curing

The crosslinking reaction of epoxy groups and hydroxy groups in PET vitrimers at fixed temperatures was measured by isothermal sweep experiments. The samples were used directly after melt compounding without curing process. The overall evolution of dynamic moduli of PET vitrimers during isothermal curing process is shown

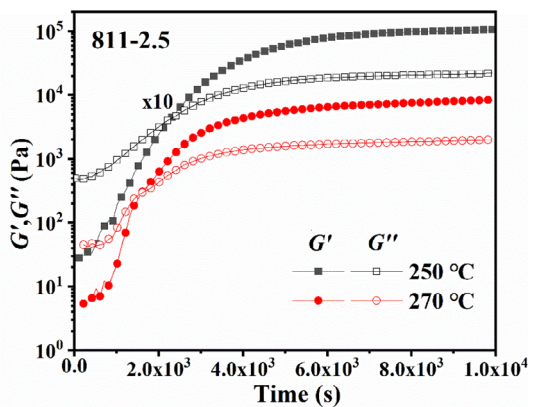


FIGURE 2 Isothermal curing process of 811-2.5 by time sweep at 250 and 270°C at a frequency of 1 Hz. (The solid lines are guided by eyes.) The data at 250°C is magnified tenfold for clarity.

in Figure 2. The early stages of moduli pattern exhibited the typical features of a sol-gel transition by gelation. Loss modulus G'' dominated the early stage of isothermal crosslinking, indicating that samples maintain uncured after melting compounding experiments, consistent with literature.³⁹ Storage modulus G' increased strongly upon time until achieving gel point where G' = G'', and exceeded G'' subsequently. It is worth noting that crossover of G' and G'' was adopted as the gel point in time sweep, but it is an apparent value instead of an accurate determination. The gel point depends on the adopted frequency, which is 1 Hz in our isothermal curing experiment. Eventually, G' reached a platform which manifested the completion of curing. By isothermal curing, uncured PET vitrimers rapidly transformed from a viscous liquid state to gel point and ultimately to an elastic solid state.

The curing process at different temperatures was performed at 250 and 270°C for comparison in 811-2.5. As expected, the moduli grew faster at 270°C due to faster reaction rate, thus reaching gel point faster at higher curing temperature. Besides, the final plateau moduli were higher for the 250°C gelation, associated with that lower temperature represents shorter observation time (higher frequency) by time-temperature equivalence principle. The final plateau moduli of 811-4.5 was an order of magnitude higher than that of 811-2.5 due to higher crosslinking degree at the same curing temperature of 270°C, as shown in the isothermal curing process in Figure S2.

However, the color of PET vitrimers became dark yellow after curing process due to oxidation and degradation as Figure S3 shows. To activate transesterification-type reaction of PET vitrimers, the curing process were required at 210°C for 72 h, which is well above T_g of epoxy-type crosslinking agent DER (~30°C). In such case, the epoxy was prone to undergo thermal oxidization

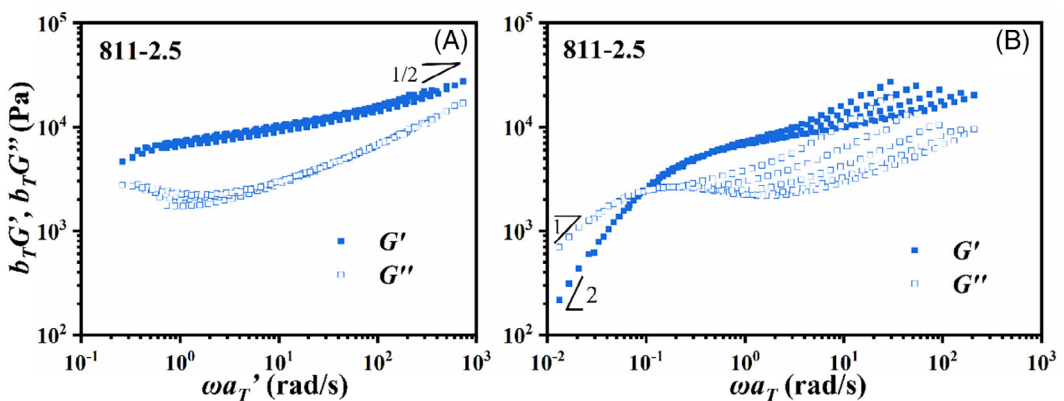


FIGURE 3 Pseudo-master curves of 811-2.5 by time-temperature superposition at $T_r = 270^\circ\text{C}$. (A) G' and G'' are shifted by a_T' at high- ω under the guidance of $b_T G''$ in the Rouse-type relaxation part at a temperature range from 270 to 300°C. (B) G' and G'' are shifted by a_T at low- ω under the guidance of $b_T G'$ in network relaxation part at a temperature range from 310 to 350°C.

and turn dark yellow.^{40,41} A similar phenomenon was also observed in previous work on epoxy-based polymers.^{42,43} Besides, the samples degraded in melt compounding without nitrogen protection, while large aromatic structures and free radicals produced in this process. However, the color change of vitrimers did not notably affect their active behaviors and thermal behaviors. To ensure that PET vitrimers were not affected by degradation, thermogravimetric analysis was conducted to characterize the thermal behavior. The TGA (Figure S4) results show that thermal behavior of PET vitrimers were improved by dynamic network without influence of oxidation. More detail data of thermal analysis in TGA are calculated in Table SI. There is no denying that oxidization and slight degradation of PET did occur, but this had negligible effect on ultimate rheological data.

3.2.2 | Time-temperature superposition

At first, amplitude sweep of vitrimers was performed to guarantee the linear viscoelasticity region as shown in Figure S5. The frequency sweep of neat PET is shown in Figure S6 for comparison at 270°C, and PET exhibited completely liquid-like behavior. Figure S7 illustrates frequency sweeps of 811-2.5 at a temperature range from 260 to 310°C. It is obvious that the plateau of storage modulus G' exhibits a downward trend at low frequency at 300°C, suggesting the onset of terminal network relaxation. Namely, transesterification reaction dominated terminal relaxation of PET vitrimers above 300°C. Thus, stress relaxation is almost contributed from the motion of Rouse-type strands below 300°C. Therefore, Figure 3A,B show pseudo-master curves of shifting frequency sweep data by the guidance of Rouse-type

relaxation and terminal network relaxation, respectively. In general, storage modulus G' and loss modulus G'' can be expressed as multiple Maxwell modes: $G'(\omega) = \sum_p g_p \frac{\omega^2 \tau_p^2}{1 + \omega^2 \tau_p^2}$ and $G''(\omega) = \sum_p g_p \frac{\omega \tau_p}{1 + \omega^2 \tau_p^2}$. $G'(\omega)$ is more sensitive to slow modes (large relaxation time τ_p), while $G''(\omega)$ is more sensitive to fast modes (small relaxation time τ_p), respectively.

On account of thermorheological complexity in dynamic covalent network (vitrimer), frequency sweep data in our work were superposed under guidance of two non-overlapped relaxation processes with a large temperature gap.³¹ Distinct molecular structures (network strands and dynamic network) in PET vitrimers are of different relaxation behaviors related to different temperature dependences. On one hand, we attempt to superpose G' and G'' data at high- ω by a factor of a_T' under the guidance of $b_T G''$, which are more sensitive to faster Rouse-type relaxation modes in glass-rubber transition. A scaling behavior of $G' \sim G'' \sim \omega^{1/2}$ at high frequency reflects Rouse-type relaxation of network strands, and rubbery plateau modulus contributed from networks can be observed in Figure 3A. On the other hand, G' and G'' data at low- ω , which are more sensitive to slow network relaxation mode, were superposed by a_T under the guidance of $b_T G'$ until reaching an agreement. Obvious scaling behavior of terminal relaxation can be seen at low- ω , namely $G' \sim \omega^2, G'' \sim \omega$, demonstrating terminal flow behavior. In summary, the whole pseudo-master curve of 811-2.5 (Figure S8) is composed of three parts: Rouse-type relaxation of network strands, rubbery plateau of network and terminal relaxation of dynamic network. To construct the pseudo-master curve, G' and G'' are multiplied by a temperature factor of $b_T = T_r/T$ ($T_r = 270^\circ\text{C}$, at which PET is in melted state) and shifted by factors of a_T and a_T' at the same time until achieving the best superposition with data at T_r . In fact,

storage modulus of PET vitrimers in this work are below 10^7 Pa, thus samples own entropic origin of rubbery part.³¹ In principle, the moduli should be modified by $b_T = \rho_r T_r / \rho T$ because G' and G'' are proportional to ρT . However, the change of density ρ with T is much smaller than the change of T itself, and can be neglected in our experiments. Thus, the vertical shift factor of PET vitrimers can be approximated as $b_T = T_r / T$.

In the panel of Figure 3A, high- ω data were superposed on the basis of G'' in high frequency, since G'' is more sensitive to fast relaxation modes. As a result, the superposition of G'' was superior to that of G' in high frequency region. At the same time, G' data in low frequency were superposed better than G'' as Figure 3B shows, owing to the sensitivity of G' to slow relaxation modes. In addition, strong failure of TTS is seen for G'' at low ω in panel a where stress relaxation is governed by network relaxation principally, which suggests that temperature dependences are different for Rouse-type relaxation and network relaxation. Meanwhile, there is a strong failure of TTS at the right side of G' in high- ω region (panel b), where modulus is mainly contributed from Rouse-type relaxation of network strands. It is worth noting that PET precursor chains are polydisperse, thus the relaxation distribution of PET vitrimers is wide. The rubbery plateau is not flat in pseudo-master curves of 811-2.5 due to polydispersity of PET. And the

precursor chains themselves have a distribution in size that widens the relaxation distribution of rubbery plateau in dynamic network. The whole relaxation process is consisted of Rouse-type relaxation of strands and dynamic network relaxation, reflecting distinct temperature dependences of different molecular structures.

Continuous relaxation spectra

The continuous relaxation spectra of 811-2.5 directly converted from frequency sweep curves were shown in Figure 4. The spectra illustrate distribution of relaxation modes in certain range of relaxation times, where the peak position is assigned to dominant relaxation time. The relaxation mode $H(\tau)$ reflects logarithmic-time-distributed modulus of system, defined as the equation:

$$G(t) = \int_0^\infty H(\tau) e^{-t/\tau} d\ln\tau \quad (1)$$

On one hand, no obvious relaxation modes are observed below 300°C because network relaxation does not start at this temperature. Besides, the observation time and relaxation scale do not match exactly due to restriction of frequency range and temperature in experiments, resulting in obscure Rouse-type relaxation peak. However, there are two trends of relaxation peaks at both ends of the spectra, indicating two different relaxation mechanisms: Rouse-type relaxation and network relaxation. On the other hand, characteristic relaxation modes are observed in relaxation spectra above 300°C, corresponding to network relaxation. The typical peaks at larger relaxation time are attributed to network relaxation, which shift to shorter time with the increase of temperature. The relaxation of PET vitrimers became faster when temperature increases, so the relaxation time of network relaxation tends to be shorter. It is demonstrated that dynamic network has been successfully introduced to PET vitrimers, resulting in two different relaxation modes. The outcomes of continuous relaxation spectra are in accordance with pseudo-master curve of 811-2.5 in Figure 3, illustrating relaxation processes with different dynamic structures clearly. The relaxation spectra further exhibit two relaxation process of PET vitrimers, including two distinct relaxation mechanisms: Rouse-type and network relaxation.

Figure 5 shows comparison of pseudo-master curves of 811-1.5 and 811-4.5 with different crosslinking density, in which both Rouse-type relaxation of network strands and network relaxation of crosslinking points can be observed. Firstly, an obvious Rouse-type scaling behavior ($G' \sim G'' \sim \omega^{1/2}$) can be observed in 811-1.5 of high- ω glass-rubber transition region, due to its lower crosslinking density. However, Rouse-type region cannot be

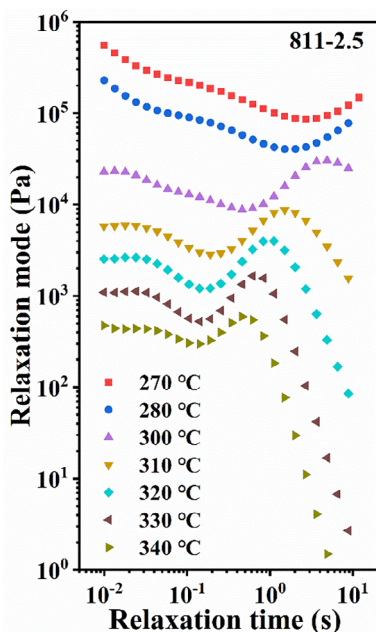


FIGURE 4 Continuous relaxation spectra $H(\tau)$ of 811-2.5 obtained from dynamic frequency sweep curves at different temperatures by Trios software. The relaxation spectra at different temperatures were magnified by different multiples in the vertical axis for clarity as shown in Table SII.

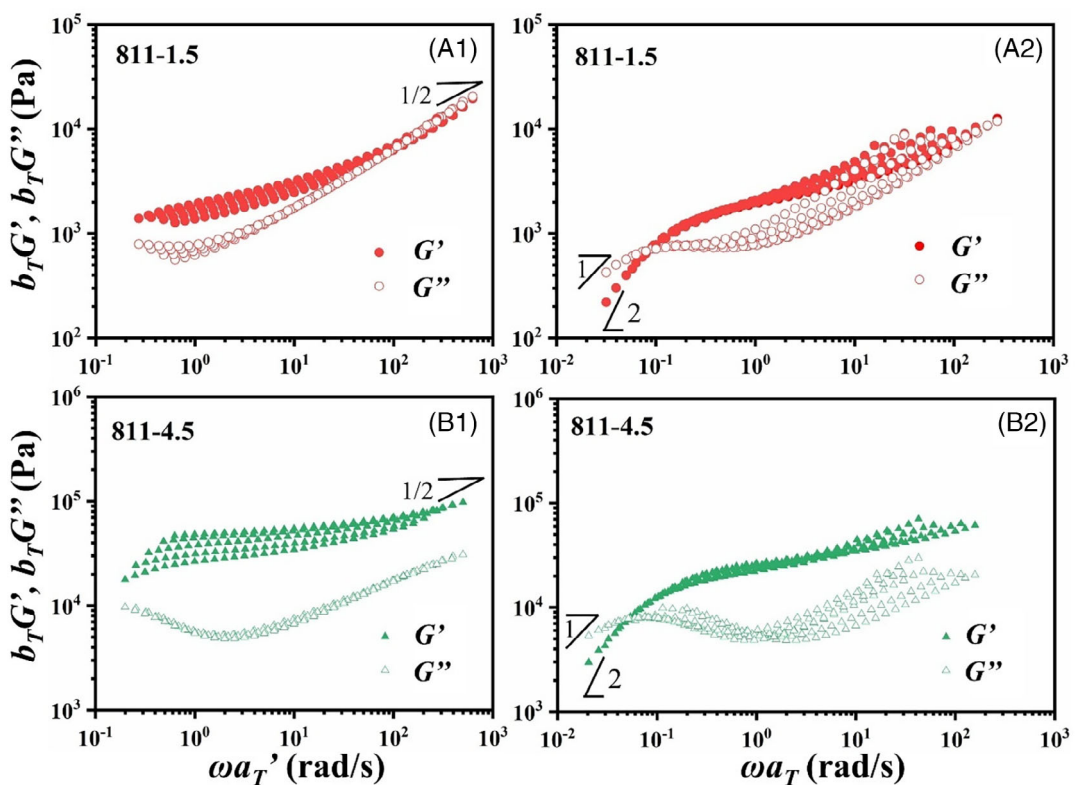


FIGURE 5 Pseudo-master curves of 811-1.5 (a1) from 270 to 300°C and (a2) from 310 to 350°C, 811-4.5 (b1) from 270 to 310°C and (b2) from 320 to 360°C by TTS at $T_f=270^\circ\text{C}$. The TTS method is the same as in Figure 3.

observed clearly in 811-2.5 and 811-4.5, when the load of crosslinking agent DER increases, corresponding to increase in crosslinking density. Namely, higher crosslinking density contributes to better established network structure, weakening the behavior of Rouse-type motion part in observation time.

The plateau modulus increased when increasing DER from 811-1.5 to 811-4.5, which is consistent with crosslinking density. Storage modulus G' was improved by more than an order of magnitude with increasing crosslink density from 811-1.5 to 811-4.5. The plateau of G' also became flatter with increase of crosslinking degree, and 811-4.5 exhibited the flattest plateau due to best established network structure. Another important transition is that terminal relaxation controlled by network dynamics shifted to lower frequency with increasing crosslinking density from 811-1.5 to 811-4.5. The details of relaxation time would be explored further in the following stress relaxation experiment part. Strong failures of TTS occurred in all PET vitrifiers, owing to distinct temperature dependences of two relaxation mechanism: Rouse-type relaxation and network relaxation. As a result of the temperature limitation to prevent degradation in PET, terminal relaxation $G' \sim \omega^2, G'' \sim \omega$ cannot be probed completely of vitrifiers in low frequency region.

It is known that the structure of PET vitrifiers is not well-defined and characterization of PET is quite difficult, whereas relaxation behavior of PET vitrimer is strongly related to dynamic network structure. On this basis, rheology is an optimal measurement for dynamics study of PET vitrifiers, which is responsive to bond exchange properties and network systems.

Shift factor – different activation energy

The horizontal (time) shift factor a'_T and a_T , which were obtained from superposing high- ω Rouse-type part of strands and low- ω network relaxation part in Figures 3 and 5, are plotted against $1000/T$ as shown in Figure 6. The appearance of two Arrhenius-type regions was associated with different temperature dependences of two relaxation mechanisms. The low temperature region (below 300°C), named Region I, is contributed from Rouse-type relaxation of network strands and the related activation energy is called flow activation energy E_a' . Otherwise, high temperature region (above 300°C) with a steeper slope is attributed to network relaxation, and the related activation energy is called reaction activation energy E_a . Flow and reaction activation energy of PET vitrifiers, E_a' and E_a , were calculated and summarized in Table 3. The transition from high to low temperatures

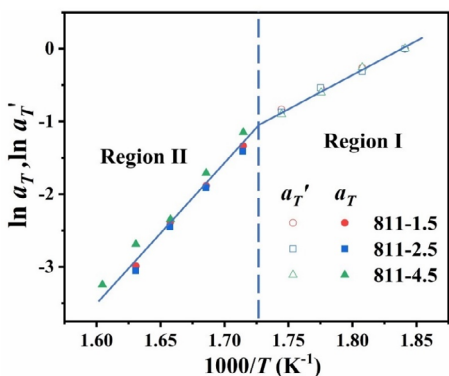


FIGURE 6 Two Arrhenius temperature dependence regions of shift factors a_T' and a_T are marked for PET vitrimer samples, Region I: flow activation energy and Region II: chemical activation energy.

indicates change of relaxation mechanism of PET vitrimers, from Rouse-type relaxation of strands to network relaxation of crosslinking points.

It is suggested that there are three regions guided mainly by distinct relaxation mechanism:⁴⁴ (1) $T_g \sim T_g + 100\text{K}$, where a WLF-type Rouse mode of precursor chain guide relaxation, but it cannot be probed below melting temperature of PET; (2) $T_g + 100\text{K} \sim T_g + 200\text{K}$, where dynamics of network strands dominate relaxation, corresponding to Region I in Figure 6; (3) $T > T_g + 200\text{K}$, where relaxation of vitrimers is principally controlled by transesterification reaction as Region II in Figure 6 shows. In particular, Region I is regarded as a diffusion dominant region contributed from terminal part of WLF-type, related to the motion of network strands. A WLF-type temperature dependence would be expected over a broad temperature range, but the relaxation time range in our work is about 4 orders of magnitude and the measuring temperature $T \gg T_g$, which is simplified to an Arrhenius type behavior finally. While Region II illustrates reaction dominant region, depending on the specificity of chemical reactions. It is confirmed that two relaxation processes are non-overlapped due to the large temperature gap between Rouse-type relaxation and network relaxation.⁴⁴ Flow activation energy E_a' shows a growing trend with increase of crosslinking degree due to restriction to chain motion, consistent with increase of T_g in Figure 1.

However, transesterification reaction of three PET vitrimers is identical, leading to nearly the same reaction activation energy E_a ($\sim 156 \text{ kJ/mol}$). The estimated E_a was within the range for the values observed in other transesterification-based vitrimers.^{30,37,45} The chemical reaction rate is associated with activation energy and temperature according to Arrhenius relation, and it is

TABLE 3 Reaction activation energy E_a and flow activation energy E_a' of PET vitrimers.

Samples	E_a (kJ/Mol)	E_a' (kJ/Mol)
811-1.5	156.3	72.0
811-2.5	157.4	73.4
811-4.5	156.3	77.5

demonstrated that our vitrimers are more sensitive to temperatures after complete curing process of 72 h. Vitrimers are supposed to own a high activation energy, so that it can act as thermosets at lower temperatures and flow like thermoplastics at high temperatures. The constructed dynamic network maybe better-defined after longer curing time, leading to larger reaction activation energy. In summary, the relaxation processes of PET vitrimers are composed of two relaxation regions, corresponding to two distinct activation energies: flow and chemical activation energy.

3.2.3 | LVE analysis

RG model—scaling comparison

At present, there is no molecular-level theory which can predict linear viscoelasticity of vitrimers exactly. In particular, theories relevant to associative polymer systems may be applied to vitrimers on account of their LVE similarity, that is, sticky-Rouse theory by Baxandall,⁴⁶ sticky-reptation theory by Leibler, Rubinstein and Colby,⁴⁷ and reversible gelation theory by Rubinstein and Semenov.⁴⁸ However, both sticky-Rouse and sticky-reptation theories take assumption of single chain mean-field picture, which means chains with the same size relax in the same way. They cannot hold near the gel point because precursor chains in sol chains and gel network exhibit completely distinct dynamic behaviors. A modified Reversible Gelation theory was developed by Chen et al. based on mean-field theory of Rubinstein and Semenov,⁴⁸ incorporating a Ginzburg transition from mean field to critical percolation.⁴⁹ The modified model can predict dynamics of ionomers such as linear viscoelasticity. Linear viscoelasticity of PET vitrimers in Figure 5 shows a similar behavior to unentangled SPS ionomer at gel point without a flat plateau.⁵⁰ It is suggested that PET vitrimers are near the gel point with low crosslink density, though exact degree of gelation and concrete fraction of sol and gel in PET vitrimers cannot be obtained, but crosslink density are calculated by plateau modulus as shown in Table 5. The purpose of this work is to analyze the structure of PET vitrimers from linear and nonlinear rheological data, which has an

excellent influence on practical applications. PET vitrimer systems are complicated dynamic network structure composed of branching agent and crosslinking agent, resulting in establishment of network (Figure S1). Thus, it is tough to determine exact gelation degree, which would produce too many fitted parameters and lead to meaningless results. In addition, associative polymers at sol-gel transition such as SPS ionomers, were described by a RG model developed by scaling approach.

On this basis, scaling analysis according to RG model is compared with dynamic behavior of PET vitrimers as shown in Figure 7. In modified RG model, the Ginzburg transition is incorporated between mean-field scaling of $G' \sim G'' \sim \omega^1$ for overlapped network strands and critical percolation scaling of $G' \sim G'' \sim \omega^{2/3}$ for nonoverlapped network strands. The scaling behavior of storage modulus G' in PET vitrimers are similar to an ionomer system slightly above gel point, where a transition appears from mean-field scaling ($G' \sim G'' \sim \omega^1$) to critical percolation scaling ($G' \sim G'' \sim \omega^{2/3}$) after Rouse relaxation. Then relaxation process was followed by rubbery plateau of network (where G'' shows a minimum) and terminal flow

relaxation ($G' \sim \omega^2$). Mean-field scaling behavior ($G' \sim G'' \sim \omega^1$) is not probed clearly in 811-2.5, which may be attributed to complicated structure and obscure master curve by different guidance of relaxation mechanisms. Critical percolation scaling ($G' \sim G'' \sim \omega^{2/3}$) is consistent with dynamic behavior observed in 811-2.5, reflecting a relaxation distribution contributed from non-overlapped gel strands with a size distribution. The subsequent plateau in 811-2.5 is not so flat as predicted from RG model, associated with the polydispersity of PET precursor chains. Terminal relaxation of dynamic network ($G' \sim \omega^2$) is obviously illustrated in low frequency region. The broad relaxation distribution of precursor generated obscure scaling of critical percolation in 811-2.5 and severe failure of TTS as discussed above in Figure 3. The scaling analysis of PET vitrimers shows an excellent fitting with RG model, which further proves the validation of rheological data in this work.

3.2.4 | Stress relaxation

Stress relaxation experiments at different temperatures were performed on PET vitrimers in the linear region at 3% strain (Figure 8). The apparent plateau modulus G_0 was selected as a normalization value where relaxation modulus was stable in Figure S9. As Figure S9 shows, the shape of curves in stress relaxation is consistent with that of pseudo-master curves in linear region, including three relaxation processes: Rouse-type relaxation of strands, rubbery plateau and terminal relaxation of network. All PET vitrimers are able to relax to $G(t) = 0$ above 270°C, demonstrating excellent dynamic properties of vitrimers. The maximum probed temperature increased upon crosslinking degree without effect of degradation, from 330°C in 811-1.5 up to 350°C in 811-4.5. The relaxation time τ_c calculated from the crossover frequency, where

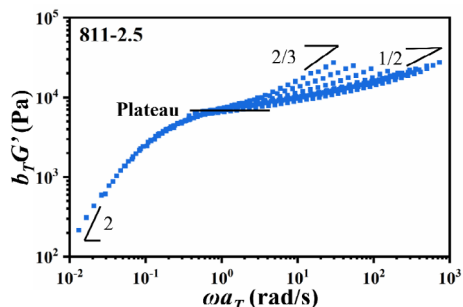


FIGURE 7 Scaling analysis of storage modulus in pseudo-master curve of 811-2.5 at low frequency based on reversible gelation model.

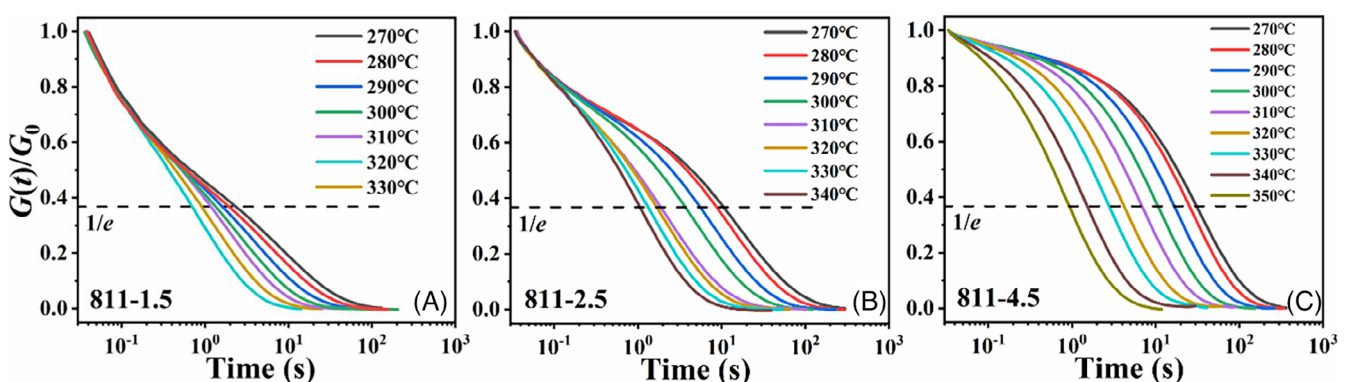


FIGURE 8 Stress relaxation curves of (A) 811-1.5, (B) 811-2.5 and (C) 811-4.5 in the temperature range between 270 and 350°C in the linear viscoelastic region.

$G'(\tau_c^{-1}) = G''(\tau_c^{-1})$ in pseudo-master curves (Figures 3 and 5) are displayed in Table 4. The data of stress relaxation were fitted to single Maxwell function $G(t) = G_0 \exp(-t/\tau_0)$ and the results are summarized in Table 4. The $1/e$ method was used to determine relaxation time $\tau_{1/e}$ (Table 4) as well, to compare the difference between relaxation of PET vitrimer and single relaxation behavior.

For individual PET vitrimer, relaxation response shifted to much shorter time scales at higher temperatures, corresponding to faster chemical reaction rate. The increase of temperature would accelerate transesterification rate of network in PET vitrimers. The rearrangement rate of network was decelerated from 811-1.5 to 811-4.5, which is attributed to more epoxy DER and higher crosslinking density of 811-4.5. In other words, the relaxation rate of network decreases with increasing crosslinking density. The values of τ_0 and $\tau_{1/e}$ are close at the same temperature because both two methods are assigned to single-exponential relaxation mechanism. However, the crossover relaxation time τ_c is quite different from the other two relaxation times below 300°C, indicating that the dynamic behavior of PET vitrimers at low temperature exist more than one relaxation mechanism. As discussed above in the part of pseudo-master curve by TTS (Figure 3), the relaxation was guided by Rouse-type motion below 300°C and network relaxation dominated the relaxation above 300°C. In addition, data could provide investigated regions with identical Weissenberg number Wi based on the terminal crossover relaxation time τ_c , which is related to transesterification reaction and chain relaxation. We note that it is rigorous to use normalized results (the same Wi) forward for nonlinear exploration, such as extensional rheology.^{51–53} As a

result, temperatures of 290, 300 and 320°C were selected for 811-1.5, 811-2.5 and 811-4.5 to carry out nonlinear experiments, respectively.

3.3 | Nonlinear rheology

3.3.1 | Extensional rheology

Figure 9 shows extensional rheology behavior for PET vitrimers at a series of extensional rates from 0.05 to 4.0 s⁻¹ with a maximum Hencky strain of 4. The inserted pictures are captured after the rupture of samples on EVF at the same extensional rate of 0.5 s⁻¹. The elongation transient viscosity η_E^+ was plotted as a function of time, and the extensional rates were increased from right to left in curves. The black line obtained from relaxation moduli in LVE region $\eta_E^+(t) = 3 \int_0^t G(\tau) d\tau$ (where zero-shear viscosity $\eta_0 = \int_0^\infty G(\tau) d\tau$) is plotted for comparison. In general, extensional data are consistent with predictions of linear viscoelasticity at low extensional rates. However, elongation viscosity η_E^+ will deviate from the value of LVE when extensional rate increases sequentially. All three PET vitrimers exhibited strain hardening

TABLE 5 The plateau modulus G_0 , molecular weight between crosslinking points M_c ($G_0 = \rho RT/M_c$), relaxation time τ_c and repairing time t_H of PET vitrimers.

Samples	G_0 (Pa)	M_c (kg/Mol)	τ_c (s)	t_H (h)
811-1.5	1765.8	3723.3	3.4	0.6
811-2.5	7231.4	909.2	4.6	1.5
811-4.5	23550.6	279.2	10.1	0.9

TABLE 4 Stress relaxation time determined from the crossover point, single Maxwell mode and $1/e$ method.

Sample	Physical quantity	Parameter						
811-1.5	Temperature (°C)	270	280	290	300	310	320	330
	τ_c (s)	7.9	6.1	4.6	3.4	2.1	1.2	0.7
	τ_0 (s)	4.2	3.4	2.5	1.9	1.5	1.1	0.8
	$\tau_{1/e}$ (s)	2.4	2.0	1.7	1.4	1.2	0.9	0.7
811-2.5	Temperature (°C)	270	280	290	300	310	320	330
	τ_c (s)	11.2	7.9	6.6	4.6	2.7	1.6	1.0
	τ_0 (s)	14.6	11.5	7.2	4.7	2.3	2.0	1.5
	$\tau_{1/e}$ (s)	10.8	8.7	5.7	3.8	1.9	1.7	1.1
811-4.5	Temperature (°C)	270	280	290	300	310	320	330
	τ_c (s)	25.1	19.3	13.7	10.1	7.9	4.5	2.4
	τ_0 (s)	31.8	25.8	17.0	11.0	7.0	4.2	2.8
	$\tau_{1/e}$ (s)	32.9	26.6	17.5	11.1	7.2	4.4	2.9

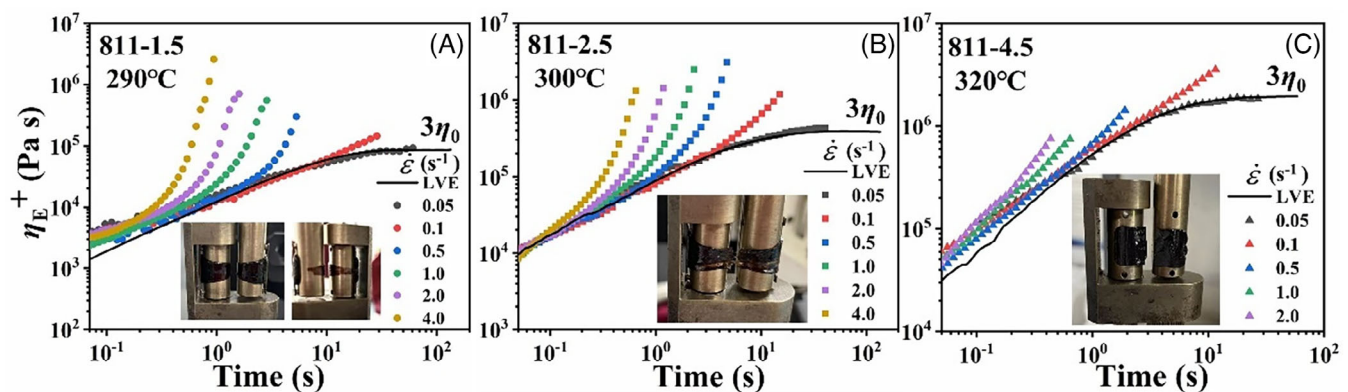


FIGURE 9 Extensional rheology behavior of (A) 811-1.5, (B) 811-2.5 and (C) 811-4.5 at 290, 300, and 320°C, respectively (η_0 is zero-shear viscosity). The inserted pictures are captured after the samples were broken on the EVF fixture at the same extensional rate.

and nonlinear characteristics due to the existence of network, while neat low-viscosity PET cannot even be stretched at all. In particular, strain hardening occurs when the observation time scale does not match relaxation time suitably, related to the degree of deviation from LVE region. The introduction of crosslinking network in PET vitrimers contributes to larger relaxation times, and the physical crosslinking points can bear more stress, resulting in strain hardening behavior. The extensional temperatures were 290, 300, and 320°C for 811-1.5, 811-2.5 and 811-4.5 to guarantee the same Weissenberg number $Wi = \dot{\epsilon}\tau_c$, determined by extensional rate and relaxation time from LVE region. It is an effective approach to compare nonlinear data more accurately.⁵¹ The elongation viscosity of all vitrimers followed LVE envelope at the extensional rate of 0.05 s⁻¹, attaining steady at larger strain. And a departure above the LVE line appears at the extensional rate of 0.1 s⁻¹ for all samples, because nonlinear rheology is based on the same Wi .

In 811-1.5, the behavior of strain hardening was enhanced with increasing extensional rate, similar to highly branched low-density polyethylenes.⁵⁴ In general, strain hardening behavior is advanced upon increasing extensional rates without exceeding the maximum strain of material. It is owing to that extensional behavior will deviate more from linear region at higher extensional rates. The elongation at break of 811-1.5 was the largest as shown in the inserted pictures in Figure 9A, indicating superior ductility of 811-1.5 vitrimer. However, 811-2.5 exhibited more obvious strain hardening at the same extensional rate (0.1 s⁻¹) compared to 811-1.5, associated with higher crosslinking density and larger relaxation time of 811-2.5.

It is interesting that 811-1.5 and 811-2.5 exhibited completely opposite trends of strain hardening. The trend of strain hardening observed in 811-2.5 resembled that of

long-chain lightly branched polymers and lightly cross-linked PEO ionomers, decreased strain hardening upon increasing extensional rate.^{51,55} This is because the strain at measurements exceeded the maximum strain of 811-2.5, leading to fracture. As inserted picture shows (Figure 9B), the elongation at break in 811-2.5 was smaller than 811-1.5, which is dependent on the ductility of material itself, indicating less ductility of 811-2.5. In other words, the maximum strain of a material is consistent with its ductility, and the maximum strain of 811-2.5 is smaller than that of 811-1.5 due to higher crosslinking degree of 811-2.5.

From 811-1.5 to 811-4.5, strain hardening became more obvious at the same shear rate of 0.1 s⁻¹, corresponding to larger relaxation time. Similar to 811-2.5, strain hardening in 811-4.5 was decreased with increasing extensional rate due to poor ductility. In addition, 811-4.5 exhibited brittle fracture with smallest elongation at break, and the extensional sample is barely stretched as inserted picture in Figure 9C. As a result, the maximum strain of 811-4.5 is smaller compared to 811-2.5 and 811-1.5. This is attributed to its highest crosslinking density and larger relaxation time of network in 811-4.5. The tensile properties of 811-4.5 is inferior to another two PET vitrimers because of less effective dynamic network, thus higher crosslinking degree is unnecessary to be explored.

So far, nonlinear behavior of dynamic covalent network (vitrimers) has not been systematically investigated in experiments. The strain hardening in PET vitrimers is more apparent compared to dissociated ionomers at small Weissenberg number, because exchange network in vitrimers is more similar to permanent crosslinked network under large extensional rate. The relaxation of network in PET vitrimers is guided by transesterification between hydroxy groups (free polyol and ring-opening of the epoxy) and ester groups from PET precursor. Thus,

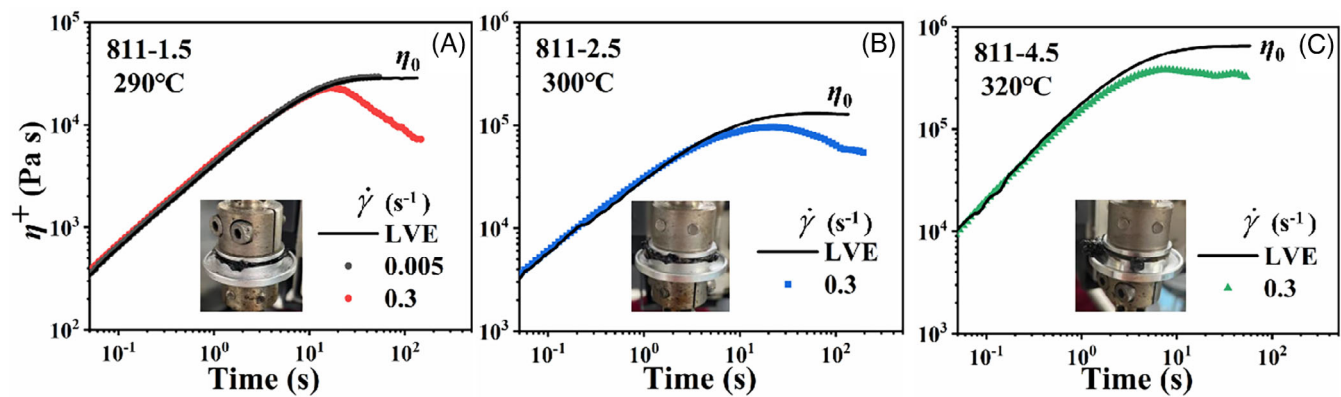


FIGURE 10 Start up shear flow of (A) 811-1.5, (B) 811-2.5 and (C) 811-4.5 at 290, 300, and 320°C, respectively (η_0 is zero-shear viscosity). Inserted pictures are captured after rapture of samples on parallel fixture.

nonlinear viscoelasticity characteristics of vitrimers are remarkable owing to the same network density during relaxation process. Consequently, PET vitrimers show more obvious nonlinear characteristics as shown in Figure 9. It is worth noting that the effect of orientation is negligible in vitrimers without dissociation, and all PET vitrimers show rigid network under extensional flow.³⁵ In summary, the ductility of PET vitrimers would decrease with increase in crosslinking degree, resulting in smaller maximum strain. Obviously, the extensional behavior of materials can be tuned by the load of crosslinking agent (network density).

3.3.2 | Start-up shear flow

Figure 10 illustrates viscosity growth function for PET vitrimers upon start-up of shear flow at various shear rates. The LVE predictions are calculated by $\eta^+(t) = \int_0^t G(\tau)d\tau$ as the solid lines. The growth of η^+ at short time follows the LVE curve irrespective of extensional rate, as linearity under small strain. $\eta^+(t)$ at low shear rates, $\dot{\gamma} = 0.005\text{ s}^{-1}$, is coincident with the LVE solid line in 811-1.5. A predicted overshoot in viscosity growth which is similar to ionomers was not observed at higher extensional rate of 0.3 s^{-1} due to edge rupture.³⁵ It is obvious that 811-1.5 underwent melt fracture at edge as shown in the inserted pictures in Figure 10A. In dissociated ionomers, η^+ at long time slightly hardens above the LVE curve at higher extensional rates, exhibits an overshoot, and then approaches the zero-shear viscosity η_0 .⁵⁰

However, all PET vitrimers went through severe melt rupture and could not flow steadily after rupture. As discussed in extensional rheology, compared to dissociated ionomers, vitrimers exhibit more obvious nonlinear behavior due to similarity to permanent

network. The network dynamics of PET vitrimers are controlled by transesterification of crosslinking points. The density of network always maintains the same during relaxation process and vitrimers exhibit distinct nonlinear characteristics. Therefore, the viscosity growth of PET vitrimers cannot be explored in our existing rheology conditions, and maybe a better fixture would be useful.

3.4 | Applications of PET vitrimers

3.4.1 | Self-repairing property

Thanks to dynamic covalent network of PET vitrimers, networks can rearrange on time scales longer than their relaxation time. This feature enables self-repairing properties of dynamic network. The self-repairing performance was quantitatively characterized via embossing repair test. It is well known that when temperature is above topology frozen temperature T_v of vitrimer, the exchange of covalent bond can allow network to relax. Vitrimers can flow during processing as thermoplastics above T_v due to the rearrangement of network topology, while they behave like thermosets below T_v . As shown in Figure 11, three PET vitrimers were embossed on the surface, by a metal ring pressed with a 2 kg weight for 5 s at 300°C (Figure S10). The surface morphologies were monitored after embossing by holding isothermal temperature for 1.5 h. All PET vitrimers' crack could be fully repaired within 1.5 h, indicating outstanding dynamic performance of network.

From data obtained from LVE frequency sweep and stress relaxation, relaxation time is extended upon increasing crosslinking degree from 811-1.5 to 811-4.5. 811-1.5 exhibited the fastest repairing property for 0.6 h, while the slowest repaired sample is 811-2.5 not 811-4.5. 811-4.5 repaired after 0.9 h, whereas 811-2.5 took 1.5 h to

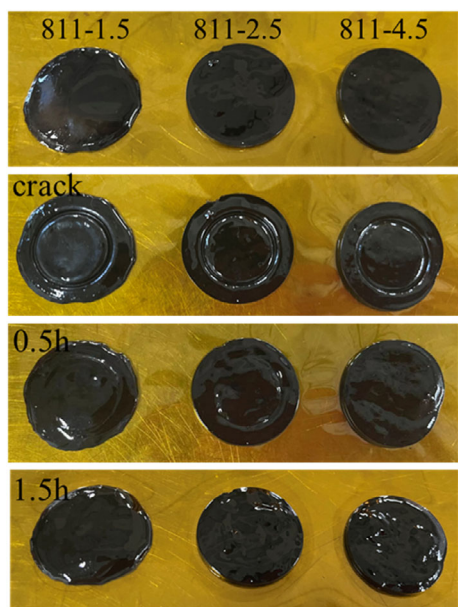


FIGURE 11 The self-repairing of surface morphology in PET vitrimers by embossing repair test within 1.5 h.

repair completely. The reason for this phenomenon is that the repairing time is determined not only by dynamic property of network, but also by the deformation resistance. In particular, deformation resistance depends on the storage modulus of samples, corresponding to plateau modulus G_0 (where G'' shows a minimum). The higher the plateau modulus of a sample, the stronger its resistance to deformation. 811-4.5 has the strongest resistance to deformation due to highest crosslinking density, which shortens its repairing time. The plateau modulus G_0 , molecular weight between crosslinking points M_c ($G_0 = \rho RT/M_c$), relaxation time τ_c and repairing time t_H are summarized in Table 5.

The introduction of network allows PET vitrimers to react by transesterification above T_v , in order to achieve self-repairing behavior. The repairing property lies on both dynamic network and deformation resistance, which is associated with bond exchange rate and plateau modulus, respectively. 811-1.5 shows the fastest exchange rate and smallest relaxation time, resulting in fastest repairing time. While the plateau modulus of 811-4.5 is higher than 811-2.5, which is contributed from higher crosslinking density, so the repairing time of 811-4.5 is shorter compared to 811-2.5. The effect of free chains on transesterification reaction has been incorporated in terminal relaxation time. Besides, The influence of temperature on dynamic bond exchange reactions may be larger than that of free chains,⁵⁶ and we focused on the effect of relaxation time that correlates with temperature. In conclusion, self-repairing properties can be adjusted by crosslinking degree of dynamic network.

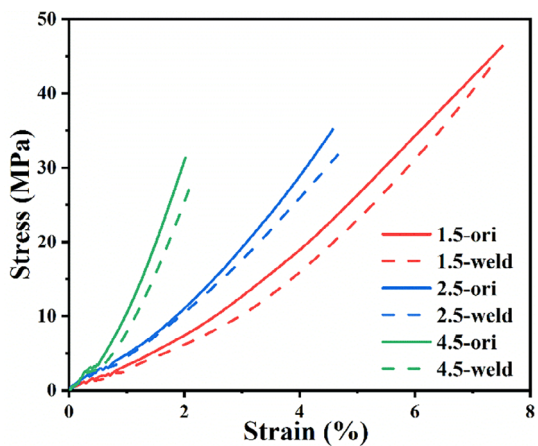


FIGURE 12 The stress–strain curves of original and welded PET vitrimers.

3.4.2 | Welding property of polymer interfaces

The welding property of PET vitrimers was also evaluated by holding isothermal temperature at 300°C for further study in Figure S11. Dumbbell-shaped samples by injection molding were used to investigate mechanical properties of PET vitrimers. At first, the dumbbell-shaped sample was cut into two pieces, and then the cut position was hot-pressed with a 5 g weight at 300°C for 5 min. Vitrimer samples were held isothermally at 300°C for 2 h for completion of welding process. It is shown that the surfaces of welded samples were quite smooth without any obvious interface after welding. When the temperature of exposed area was high enough (above T_v) to activate transesterification, the two pieces were welded together within 2 h. To analyze welding properties of PET vitrimers quantitatively, stress–strain curves of original and welded PET vitrimers are displayed in Figure 12. The results showed that mechanical properties of PET vitrimers were nearly recovered without losing any mechanical properties, only a small loss part may result from thermal degradation. The degradation of PET would be caused by prolonged exposure to high temperatures without nitrogen protection. Thus, excellent welding properties of PET vitrimers may provide potential opportunities to satisfy some special requirements for welding application.

Moreover, stress–strain curves of three PET vitrimers are consistent with extensional rheology experiments, indicating ductility or brittleness of materials. 811-1.5 exhibited the largest elongation at break, arising from its excellent ductility. The lowest crosslinking density of network contributes to best ductility for 811-1.5 compared to the other two vitrimers. While 811-4.5 exhibited the highest Young's modulus and behave like a brittle material

due to its high crosslinking density. The Young's modulus was enhanced with increasing crosslinking degree, whereas the elongation at break was decreased from 811-1.5 to 811-4.5. As well, the mechanical properties are determined by crosslinking density of network.

4 | CONCLUSION

In present work, dynamic covalent network was introduced to PET to transform it to PET vitrimer with different crosslink density, thus combining the advantages of thermoplastics and thermosets. The crosslinking points can offer heterogeneous nucleation sites for PET or act as a physical barrier for chain packing, depending on the degree of crosslinking. The rheological data are sensitive to dynamic network and bond exchange mechanism in PET vitrimers. The pseudo-master curve by TTS shows that relaxation processes of PET vitrimers can be divided to three parts: Rouse-type relaxation of network strands, rubbery plateau and terminal relaxation of dynamic network, consistent with reversible gelation model. Flow activation energy obtained by TTS exhibits a growing trend as crosslinking degree increases, while chemical reaction activation energy shows similar results. As degree of crosslinking increases, the relaxation time of dynamic network becomes larger. In addition, all PET vitrimers exhibit apparent strain hardening behavior in nonlinear rheology, but extensional flow characteristics of vitrimers are quite distinct. The strain hardening of 811-1.5 was enhanced with increasing extensional rate, opposite to the trends of 811-2.5 and 811-4.5. The ductility of samples decreases upon increasing crosslinking density and can be adjusted according to industrial demands. Owing to dynamic network, PET vitrimers show outstanding self-repairing and welding properties with significant potentials and guiding importance in engineering plastics.

ACKNOWLEDGMENTS

The authors thank the financial support from the National Natural Science Foundation of China (grant no. 21973017, 21774027, and 21534002).

CONFLICT OF INTEREST STATEMENT

The authors declare no competing financial interest.

ORCID

Ping Tang  <https://orcid.org/0000-0003-0253-1836>

REFERENCES

- [1] L. Xie, Y. Xie, Q. Wu, M. Wang, Q. Wu, X. Zhou, X. Ge, *Ind. Eng. Chem. Res.* **2015**, *54*, 4748.
- [2] K. Nomura, X. Peng, H. Kim, K. Jin, H. J. Kim, A. F. Bratton, C. R. Bond, A. E. Broman, K. M. Miller, C. J. Ellison, *ACS Appl. Mater. Interfaces* **2020**, *12*, 9726.
- [3] B. A. Pulido, O. S. Habboub, S. L. Aristizabal, G. Szekely, S. P. Nunes, *ACS Appl. Polym. Mater.* **2019**, *1*, 2379.
- [4] A. M. Ahmed, T. P. Kainulainen, J. P. Heiskanen, *Ind. Eng. Chem. Res.* **2021**, *60*, 7495.
- [5] S. Yoshida, K. Hiraga, T. Takehana, I. Taniguchi, H. Yamaji, Y. Maeda, K. Toyohara, K. Miyamoto, Y. Kimura, K. Oda, *Science* **2016**, *351*, 1196.
- [6] S. Joo, I. J. Cho, H. Seo, H. F. Son, H.-Y. Sagong, T. J. Shin, S. Y. Choi, S. Y. Lee, K.-J. Kim, *Nat. Commun.* **2018**, *9*, 382.
- [7] R. P. Choudhury, J. S. Lee, R. M. Kriegel, W. J. Koros, H. W. Beckham, *Macromolecules* **2012**, *45*, 879.
- [8] H. Gao, Y. Bai, H. Liu, J. He, *Ind. Eng. Chem. Res.* **2019**, *58*, 21872.
- [9] M. Kruse, P. Wang, R. S. Shah, M. H. Wagner, *Polym. Eng. Sci.* **2019**, *59*, 396.
- [10] M. Härtl, A. Dörnhöfer, *Polymer* **2020**, *12*, 1605.
- [11] Y. Ge, S. Yao, M. Xu, L. Gao, Z. Fang, L. Zhao, T. Liu, *Ind. Eng. Chem. Res.* **2019**, *58*, 3666.
- [12] Z. J. Wang, J. G. Wang, Y. Y. Pang, J. Zhu, W. E. Zheng, *Polymer* **2022**, *254*, 254.
- [13] W. Zhang, H. B. Zhang, L. P. Yang, Y. Tang, P. Tang, *J. Ind. Eng. Chem.* **2022**, *109*, 510.
- [14] S. Dong, Y. Jia, X. Xu, J. Luo, J. Han, X. Sun, *J. Colloid Interface Sci.* **2019**, *539*, 54.
- [15] J. W. Gilmer, R. P. Neu, Y. J. Liu, A. K. Y. Jen, *Polym. Eng. Sci.* **1995**, *35*, 1407.
- [16] W. Zhang, H. Zhang, Y. Yang, P. Tang, *Polym. Bull.* **2022**, *79*, 3803.
- [17] S. L. Xing, R. Li, J. J. Si, P. Tang, *J. Ind. Eng. Chem.* **2016**, *38*, 167.
- [18] S. L. Xing, P. Tang, Y. L. Yang, *J. Appl. Polym. Sci.* **2015**, *132*, 41240.
- [19] S. Xing, R. Li, P. Tang, *Macromol. Chem. Phys.* **2015**, *216*, 301.
- [20] J. Qiu, S. Ma, S. Wang, Z. Tang, Q. Li, A. Tian, X. Xu, B. Wang, N. Lu, J. Zhu, *Macromolecules* **2021**, *54*, 703.
- [21] D. Montarnal, M. Capelot, F. Tournilhac, L. Leibler, *Science* **2011**, *334*, 965.
- [22] T. Liu, C. Hao, S. Zhang, X. Yang, L. Wang, J. Han, Y. Li, J. Xin, J. Zhang, *Macromolecules* **2018**, *51*, 5577.
- [23] Z. Feng, J. Hu, H. Zuo, N. Ning, L. Zhang, B. Yu, M. Tian, *ACS Appl. Mater. Interfaces* **2019**, *11*, 1469.
- [24] A. Legrand, C. Soulié-Ziakovic, *Macromolecules* **2016**, *49*, 5893.
- [25] Z. Wang, H. Tian, Q. He, S. Cai, *ACS Appl. Mater. Interfaces* **2017**, *9*, 33119.
- [26] R. Martin, A. Rekondo, A. Ruiz De Luzuriaga, G. Cabañero, H. J. Grande, I. Odriozola, *J. Mater. Chem. A* **2014**, *2*, 5710.
- [27] D. J. Fortman, R. L. Snyder, D. T. Sheppard, W. R. Dichtel, *ACS Macro Lett.* **2018**, *7*, 1226.
- [28] M. Rottger, T. Domenech, R. van der Weegen, A. B. R. Nicolay, L. Leibler, *Science* **2017**, *356*, 62.
- [29] A. Demongeot, R. Groote, H. Goossens, T. Hoeks, F. Tournilhac, L. Leibler, *Macromolecules* **2017**, *50*, 6117.
- [30] M. Hayashi, R. Yano, *Macromolecules* **2020**, *53*, 182.
- [31] S. Wu, H. Yang, W.-S. Xu, Q. Chen, *Macromolecules* **2021**, *54*, 6799.

- [32] N. Jiang, H. Zhang, P. Tang, Y. Yang, *Macromolecules* **2020**, 53, 3438.
- [33] N. Jiang, H. Zhang, Y. Yang, P. Tang, *J. Rheol.* **2021**, 65, 527.
- [34] J. Shao, N. Jiang, H. Zhang, Y. Yang, P. Tang, *Macromolecules* **2022**, 55, 535.
- [35] X. Cui, N. Jiang, J. Shao, H. Zhang, Y. Yang, P. Tang, *Macromolecules* **2023**, 56, 772.
- [36] Z. Zhang, C. Huang, R. A. Weiss, Q. Chen, *J. Rheol.* **2017**, 61, 1199.
- [37] Y. Zhou, J. G. P. Goossens, R. P. Sijbesma, J. P. A. Heuts, *Macromolecules* **2017**, 50, 6742.
- [38] G. P. Kar, M. O. Saed, E. M. Terentjev, *J. Mater. Chem. A* **2020**, 8, 24137.
- [39] H. Fang, W. Ye, Y. Ding, H. H. Winter, *Macromolecules* **2020**, 53, 4855.
- [40] X. Kuang, G. Liu, X. Dong, X. Liu, J. Xu, D. Wang, *J. Polym. Sci., Part A: Polym. Chem.* **2015**, 53, 2094.
- [41] Q. Shi, K. Yu, X. Kuang, X. Mu, C. K. Dunn, M. L. Dunn, T. Wang, H. J. Qi, *Mater. Horiz.* **2017**, 4, 598.
- [42] Y. Min, S. Huang, Y. Wang, Z. Zhang, B. Du, X. Zhang, Z. Fan, *Macromolecules* **2015**, 48, 316.
- [43] Q. Shi, K. Yu, M. L. Dunn, T. Wang, H. J. Qi, *Macromolecules* **2016**, 49, 5527.
- [44] L. E. Porath, C. M. Evans, *Macromolecules* **2021**, 54, 4782.
- [45] T. Isogai, M. Hayashi, *Macromolecules* **2022**, 55, 6661.
- [46] L. G. Baxandall, *Macromolecules* **1982**, 1989, 22.
- [47] L. Leibler, M. Rubinstein, R. H. Colby, *Macromolecules* **1991**, 24, 4701.
- [48] M. Rubinstein, A. N. Semenov, *Macromolecules* **1998**, 31, 1386.
- [49] Q. Chen, C. Huang, R. A. Weiss, R. H. Colby, *Macromolecules* **2015**, 48, 1221.
- [50] C. Huang, Q. Chen, R. A. Weiss, *Macromolecules* **2016**, 49, 9203.
- [51] A. Shabbir, Q. Huang, G. P. Baeza, D. Vlassopoulos, Q. Chen, R. H. Colby, N. J. Alvarez, O. Hassager, *J. Rheol.* **2017**, 61, 1279.
- [52] S. Liu, Z. Zhang, Q. Chen, Y. Matsumiya, H. Watanabe, *Macromolecules* **2021**, 54, 9724.
- [53] S. Liu, Y. Zhang, Z. Zhang, Q. Chen, *J. Rheol.* **2022**, 66, 1.
- [54] M. H. Wagner, M. Yamaguchi, M. Takahashi, *J. Rheol.* **2003**, 47, 779.
- [55] C. Gabriel, H. Münstedt, *J. Rheol.* **2003**, 47, 619.
- [56] J. Wu, S. Li, H. Liu, H. Qian, Z. Lu, *Phys. Chem. Chem. Phys.* **2019**, 21, 13258.

SUPPORTING INFORMATION

Additional supporting information can be found online in the Supporting Information section at the end of this article.

How to cite this article: W. Zhang, X. Cui, H. Zhang, Y. Yang, P. Tang, *J. Polym. Sci.* **2023**, 1, <https://doi.org/10.1002/pol.20230169>